INFRAGRAVITY VELOCITY PROFILES IN THE SURF-ZONE

UDAY PUTREVU and IB A. SVENDSEN

RESEARCH REPORT NO. CACR-94-10

February 1994

CENTER FOR APPLIED COASTAL RESEARCH

Ocean Engineering Laboratory
University of Delaware
Newark, Delaware 19716

Infragravity Velocity Profiles in the Surf-Zone

Uday Putrevu and Ib A. Svendsen

Center for Applied Coastal Research, Department of Civil Engineering

University of Delaware, Newark, DE 19716

Abstract

The vertical structure of the velocity profiles in infragravity waves is analyzed. It is shown that while the velocity under free infragravity waves does not vary significantly with the vertical coordinate, the velocity under forced infragravity waves has a substantial vertical structure. The dispersion coefficient (caused by the vertical variations of the velocities in steady currents and infragravity waves) which plays an important role in determining the horizontal structure of currents and infragravity waves in the nearshore region is found to have substantial temporal variation. This temporal variation will contribute to the generation of higher harmonics of infragravity waves. Additionally, it is found that under forced infragravity waves the nondimensional horizontal dispersion coefficient will have substantial spatial variations.

1 Introduction

The first observations of infragravity waves in the nearshore region were reported by Munk (1949) and Tucker (1950). They coined the term "surf beats" to describe phenomena with periods in the range of two to five minutes. Their observations suggested that the infragravity waves were correlated with the group structure of the waves. Recent field observations (Huntley *et al.* 1981; Wright *et al.* 1982; Guza & Thornton 1982, 1985; Oltman-Shay & Guza 1987; Howd *et al.* 1991 to mention a few) have shown that there is significant energy present at infragravity frequencies in the surf-zone. In some cases the energy at infragravity frequencies exceeds the energy present at the short wave frequencies (Wright *et al.* 1982, Guza & Thornton 1982).

Longuet-Higgins & Stewart (1962, 1964) showed that groups of unbroken short waves could force a long wave at the group period and suggested that these so called bound long waves are (partly) released at the break point, propagate to the beach where they are reflected at the coast and propagate back out as free long waves. However, the energy content of bound long waves is insufficient to account for the observations of significant infragravity energy found in recent field observations. For example, Herbers *et al.* (1992) measured the infragravity energy outside the surf-zone and found it to be much higher than the predictions of bound long waves and concluded that infragravity waves generated in the surf-zone and radiated out are frequently the dominant source of energy in the infragravity band (see also Elgar *et al.* 1992).

Symonds *et al.* (1982) and Schaffer & Svendsen (1988) proposed mechanisms for the generation of infragravity waves in the surf-zone due to breaking of wave groups. Symonds *et al.* assumed that since the individual waves in a group have different wave heights they will break at different locations thereby causing a time variation of the break point position. They further assumed that all the groupiness of the incident wave field is destroyed by the breaking process. Their results showed that the time variation of the break point generates long waves at the group period and its higher harmonics. The lack of groupiness in the surf-zone implies that no further long wave generation takes place there and all the long wave motion inside the surf-zone consists entirely of free long waves. They also showed that for typical parameter values the higher harmonics are much smaller than the fundamental.

Schaffer & Svendsen (1988) considered the other extreme situation assuming that all the waves in a group broke at a fixed location. This implies that the group structure of the incident wave field is transmitted into the surf-zone. Their results showed that the groups of broken waves continue the generation of long waves at the group period. The long wave motion in the surf-zone becomes a combination of free and forced long waves. Recently Schaffer (1993) combined the models of Symonds *et al.* (1982) and Schaffer & Svendsen (1988) to allow for a time variation of the break point as well as a partial transmission of the group structure into the surf-zone.

The works cited in the last two paragraphs started with the depth integrated shallow water equations averaged over a wave period as given, *e.g.*, by Phillips (1977) or Mei (1983). These equations do not allow for a vertical variation of the short-wave-averaged horizontal velocity. In the present paper we determine the vertical variation of the horizontal velocity under infragravity

waves. For simplicity, we limit the analysis to the 2D case of surf-beats (no alongshore variation) caused by periodic wave groups. The approach used is analogous to the approach used to determine the vertical structure nearshore currents (Svendsen & Lorenz 1989, Svendsen & Putrevu 1990) where the Reynolds averaged equations of horizontal momentum are solved to determine the local vertical structure of nearshore currents. Although the situations considered are rather different, the approach also has similarities with the works of Davies (1987) and Jin & Kranenburg (1993).

Using this approach Putrevu & Svendsen (1992) and Svendsen & Putrevu (1993) demonstrated that, in the steady case, the interaction of the cross-shore and longshore currents can be represented by a dispersive term. This term was found to be ten to fifty times stronger than the lateral mixing caused by the breaker turbulence and to completely control the cross-shore structure of longshore currents. This effect, which has been completely neglected in all previous work, would clearly be an important element in the general 3D case in modifying the horizontal distribution of currents and infragravity wave motions such as edge waves. For that reason, the temporal variation of the dispersion coefficient is analyzed here.

The paper is organized in the following fashion. Section 2 states the equations governing the short-wave-averaged velocity in the nearshore region. In section 3 we solve for the local vertical structure of periodic infragravity motion. The numerical results for the infragravity velocity profiles and the resulting temporal variations of the dispersion coefficient alluded to above are presented in section 4. The work is summarized and the major conclusions are restated in section 5.

2 Governing Equations

We consider the situation on a gently sloping long straight coast with no alongshore variations. Furthermore, we restrict ourselves to shallow water so that the pressure variation in the long waves is hydrostatic under the free surface. We also note that in the short-wave-averaged approach used here, the infragravity wave motion is entirely equivalent to a time varying current. The appropriate equations can therefore be deduced from the general equations derived by Svendsen & Lorenz (1989). Under the conditions indicated, the depth variations of the cross-shore and

longshore components of the short-wave-averaged velocity are governed by

$$\frac{\partial U}{\partial t} - \frac{\partial}{\partial z}\left(\nu_t \frac{\partial U}{\partial z}\right) = -g\frac{\partial \overline{\zeta}}{\partial x} - \overline{u_w \frac{\partial u_w}{\partial x}} \tag{1}$$

and

$$\frac{\partial V}{\partial t} - \frac{\partial}{\partial z}\left(\nu_t \frac{\partial V}{\partial z}\right) = -\overline{u_w \frac{\partial v_w}{\partial x}} - U\frac{\partial V_m}{\partial x} \tag{2}$$

Here the turbulent correlations have been parameterized by an eddy viscosity ν_t, $U(x,z,t)$ and $V(x,z,t)$ represent the short-wave-averaged velocities, V_m represents the depth averaged value of V, u_w and v_w represent the short wave induced velocity components in the cross-shore (x) and longshore (y) directions. In (1), (2) and all subsequent equations an overbar denotes a quantity averaged over a short wave period. $\overline{\zeta}$ is the short-wave-averaged free surface elevation (equivalent to the surface elevation in the infragravity waves superposed on the steady set-up). $\overline{\zeta}$ would essentially be determined by the continuity equation

$$\frac{\partial \overline{\zeta}}{\partial t} + \frac{\partial Q}{\partial x} = 0 \tag{3}$$

where Q is the volume flux in the cross-shore direction.

Equations 1 and 2 represent extensions to the time varying situation for the usual equations governing the undertow and longshore currents. Starting from the equations given in Svendsen & Lorenz (1989), the arguments leading up to (1) and (2) for the steady case (including the justification for using V_m in the interaction term in (2)) were given in Putrevu & Svendsen (1993) and Svendsen & Putrevu (1993) respectively.

In the latter publication, we also derived the equation governing the steady state cross-shore distribution of the longshore current. The extension of that equation to the unsteady case is

$$-\frac{\partial (hV_m)}{\partial t} + \frac{\partial}{\partial x}\left[(\nu_t + D_c)\, h\frac{\partial V_m}{\partial x}\right] - \frac{\tau_{by}}{\rho} - \frac{\partial}{\partial x}(F_2 V_m) = \frac{1}{\rho}\frac{\partial S_{xy}}{\partial x} + \frac{\partial F_1}{\partial x} \tag{4}$$

where the terms containing D_c, F_1 and F_2 represent dispersion which arises from the nonlinear interaction of the longshore and cross-shore short-wave-averaged velocities. It was found that the dispersive mixing represented by the D_c term controls the cross-shore distribution of the longshore current, exceeding the contribution from the turbulent mixing (represented by the ν_t term) by at least an order of magnitude. D_c is given by

$$D_c = \frac{1}{h}\int_{-h_0}^{\overline{\zeta}} U \int_z^{\overline{\zeta}} \frac{1}{\nu_{tz}} \int_{-h_0}^{z} U \, dz \, dz \, dz \tag{5}$$

Equation 4 shows that temporal variations in D_c (which in the case of longshore uniformity considered here are caused by temporal variations in U) may be important and will generate higher harmonics in V_m. The temporal variation of U is governed by (1) which is solved for periodic infragravity motion in the next section.

3 Solution for Periodic Infragravity Motions

3.1 Boundary Conditions

In general, the solution of (1) requires the specification of appropriate initial conditions and two boundary conditions. In this paper, we restrict ourselves to periodic infragravity motions and thereby eliminate the need for initial conditions.

As one boundary condition we relate the bottom shear stress to the velocity profile

$$\rho\nu_t\frac{\partial U}{\partial z}\Big)_{z=-h_0} = \tau_b \tag{6}$$

and assume that the bed shear stress is related to the near bottom velocity $U_b = U(z = -h_0)$ by

$$\tau_b = \frac{1}{2}\rho f_w u_0 U_b \tag{7}$$

where f_w is a friction factor and u_0 is the amplitude of the near bottom short-wave induced oscillatory velocity. (6) and (7) lead to the following boundary condition for the velocity profile (Svendsen & Hansen 1988)

$$\nu_t\frac{\partial U}{\partial z}\Big)_{z=-h_0} = \frac{1}{2}f_w u_0 U_b \tag{8}$$

For the steady case, most undertow solutions specify the depth integrated volume flux as a second boundary condition. For the time varying case considered here the phase of the depth integrated volume flux will, in general, be different from the phase of the forcing represented by the RHS of (1). In a complete solution, the time variation of the depth integrated volume flux would be deduced from an equation analogous to (4) in the cross-shore direction in combination with the continuity equation. This step constitutes determining the long wave pattern (see, *e.g.*, Symonds *et al.* 1982, Symonds & Bowen 1984, Schaffer & Svendsen 1988, List 1992, Schaffer 1993). Here we assume that this pattern is known and focus on analyzing the local variation

of the infragravity velocity profiles. However, unless we include an evolution of the long wave pattern, we will not know the phase relationship between the forcing and the volume flux in advance. Therefore, instead of the depth integrated volume flux, we use as the second boundary condition the shear stress τ_s at the mean water level. This τ_s (discussed further in section 4) is related to the slope of the vertical profile of the velocity to form the second boundary condition

$$\rho\nu_t\frac{\partial U}{\partial z}\Big)_{z=\overline{\zeta_0}} = \tau_s \tag{9}$$

where $\overline{\zeta_0}$ is the steady mean water surface (see figure 1).

3.2 Solution Procedure

The short-wave-averaged quantities in the surf-zone such as cross-shore currents and set-up may be separated into steady and unsteady parts as

$$f(x,z,t) = f_0(x,z) + f_1(x,z,t) \tag{10}$$

where the subscripts 0 and 1 refer to the steady and unsteady (infragravity) parts respectively. For example, the steady set-up $\overline{\zeta_0}$ corresponds to the set-up caused by the mean short-wave motion, the unsteady part $\overline{\zeta_1}$ to the set-up caused by the short wave modulation (the wave groupiness). As indicated earlier, this time varying set-up essentially represents the surface elevation due to the infragravity wave motion. The same applies to the velocity U and the surface shear stress τ_s.

Substituting (10) into (1) and separating into steady and unsteady parts leads to

$$\frac{\partial}{\partial z}\left(\nu_t\frac{\partial U_0}{\partial z}\right) = g\frac{d\overline{\zeta_0}}{dx} + \left(\overline{u_w\frac{\partial u_w}{\partial x}}\right)_0 \tag{11}$$

and

$$\frac{\partial U_1}{\partial t} - \frac{\partial}{\partial z}\left(\nu_t\frac{\partial U_1}{\partial z}\right) = -g\frac{d\overline{\zeta_1}}{dx} - \left(\overline{u_w\frac{\partial u_w}{\partial x}}\right)_1 \tag{12}$$

The corresponding boundary conditions are

At mean water level ($z = \overline{\zeta_0}$)

$$\nu_t\frac{\partial U_0}{\partial z} = \frac{\tau_{s,0}}{\rho} \tag{13}$$

$$\nu_t\frac{\partial U_1}{\partial z} = \frac{\tau_{s,1}}{\rho} \tag{14}$$

At the bottom ($z = -h_0$)

$$\nu_t \frac{\partial U_0}{\partial z} = \frac{1}{2} f_w u_0 U_{0b} \tag{15}$$

$$\nu_t \frac{\partial U_1}{\partial z} = \frac{1}{2} f_w u_0 U_{1b} \tag{16}$$

Equation 11 subject to (13) and (15) is the usual undertow problem inside the surf-zone. The solution to this problem has been analyzed extensively in the literature (Svendsen 1984, Dally & Dean 1984, deVriend & Stive 1987, Svendsen *et al.* 1987, Roelvink & Stive 1988, Svendsen & Hansen 1988 and Okayasu *et al.* 1988 to mention a few) and will be assumed known and not discussed further here. For the rest of this section, we will concentrate on solving (12) subject to (14) and (16) which means determining the vertical variation of the velocity for infragravity wave motion.

In (14) the term $\tau_{s1}(x,t)$ in the surface boundary condition represents the time and space variation above the mean water level of the radiation stress due to the wave groupiness. Similarly, in (12) the $\overline{(u_w \partial u_w/\partial x)_1}$ term represents the variation of the radiation stress between the bottom and the mean water level. Hence, both these terms are in phase with the short wave height variation. In contrast, the $\partial\overline{\zeta_1}/\partial x$ term in (12) represents the surface elevation gradient in the long wave motion which, in general, will not be in phase with (or even phase locked to) the short wave height variation.

Since the problem is linear and we consider periodic wave groups the infragravity components of the motion may be expressed as

$$U_1(x,z,t) = U_a(x,z)\exp(-i\omega t) \tag{17}$$

$$\zeta_1(x,t) = b_a \exp(-i\omega t) \tag{18}$$

$$\tau_{s,1}(x,t) = T_1(x,t)\exp(-i\omega t) \tag{19}$$

$$\overline{u_{w1}^2} = U_w^2(x)\exp(-i\omega t) \tag{20}$$

$$-g\frac{d\overline{\zeta_1}}{dx} - \left(\overline{u_w \frac{\partial u_w}{\partial x}}\right)_1 = F_1(x)\exp(-i\omega t) \tag{21}$$

where U_a, b_a, T_1, U_w and F_1 are in general complex. In (21) F_1 does not depend on the vertical coordinate because the shallow water assumption for the short waves implies that u_w does not depend on depth (except in the boundary layer at the bottom).

Substituting the above into (12) gives

$$\frac{\partial^2 U_a}{\partial z^2} + \frac{i\omega}{\nu_t} U_a = \frac{F_1}{\nu_t} \tag{22}$$

subject to

$$\nu_t \frac{\partial U_a}{\partial z}\Big)_{z=\overline{\zeta_0}} = \frac{T_1}{\rho} \tag{23}$$

and

$$\nu_t \frac{\partial U_a}{\partial z}\Big)_{z=-h_0} = \frac{1}{2} f_w u_0 U_a(z=-h_0) \tag{24}$$

A direct solution of (22) subject to (23) and (24) is mathematically straightforward. It is done here by splitting U_a into three parts U_{a1}, U_{a2} and U_{a3} as follows:

$\underline{U_{a1}}$

$$U_{a1} = \frac{F_1}{i\omega} \tag{25}$$

which represents the the depth uniform response to the depth uniform forcing.

$\underline{U_{a2}}$

$$\frac{\partial^2 U_{a2}}{\partial z^2} + \frac{i\omega}{\nu_t} U_{a2} = 0 \tag{26}$$

subject to

$$\nu_t \frac{\partial U_{a2}}{\partial z}\Big)_{z=\overline{\zeta}_0} = \frac{T_1}{\rho} \tag{27}$$

and

$$\nu_t \frac{\partial U_{a2}}{\partial z}\Big)_{z=-h_0} = 0 \tag{28}$$

Thus, U_{a2} is the velocity component forced by the surface shear stress.

$\underline{U_{a3}}$

$$\frac{\partial^2 U_{a3}}{\partial z^2} + \frac{i\omega}{\nu_t} U_{a3} = 0 \tag{29}$$

subject to

$$\nu_t \frac{\partial U_{a3}}{\partial z}\Big)_{z=\overline{\zeta}_0} = 0 \tag{30}$$

and

$$\nu_t \frac{\partial U_{a3}}{\partial z}\Big)_{z=-h_0} = \frac{1}{2} f_w u_0 \left(U_{a1} + U_{a2}(z=-h_0) + U_{a3}(z=-h_0)\right) \tag{31}$$

U_{a3} is forced by the bed shear stress. It is easily verified that the total solution for U_a is the linear superposition of U_{a1}, U_{a2} and U_{a3}.

If we let

$$F_1 = F_a \exp(-i\alpha) \tag{32}$$

$$T_1 = T_s \exp(-i\delta) \tag{33}$$

the solutions for U_{r1}, U_{r2} and U_{r3} (representing the real parts of $U_{aj}\exp(-i\omega t)$) are (see appendix for details)

$$U_{r1} = \frac{F_a}{\omega}\cos(\omega t) \tag{34}$$

$$U_{r2} = \frac{F_a}{\omega}\left\{\frac{\sqrt{2}T_s\beta}{\rho F_a}F_2(z)\cos[\omega t - \phi_B - \phi_{z2}(z)]\right\} \tag{35}$$

$$U_{r3} = \frac{F_a}{\omega}\left\{\frac{f_w u_0}{2\nu_t\beta}\frac{\omega}{F_a}U_{1b}F_3(z)\cos[\omega t - \phi_D - \phi_3(z)]\right\} \tag{36}$$

where the various quantities are defined in the appendix. The parameter

$$\beta = \sqrt{\frac{\omega}{2\nu_t}} \tag{37}$$

is analogous to the parameter encountered in the solution for wave boundary layers (Longuet-Higgins 1953). The total solution for U_1 is then given by

$$U_1 = \frac{F_a}{\omega}\left\{\cos(\omega t) + \frac{\sqrt{2}T_s\beta}{\rho F_a}F_2(z)\cos[\omega t - \phi_B - \phi_{z2}(z)] + \frac{f_w u_0}{2\nu_t\beta}\frac{\omega}{F_a}U_{1b}F_3(z)\cos[\omega t - \phi_D - \phi_3(z)]\right\} \tag{38}$$

In the above $t = 0$ is chosen to correspond to the maximum value of U_{r1}.

4 Results for the Velocity Profiles

4.1 Parameter Values

In view of the many parameters that turn out to influence the temporal variation of the vertical profiles, the most illustrative approach for examining the results is to select two typical situations and choose the parameter values based on a quantitative estimate of their general magnitude. An analysis of (38) (see appendix) reveals that the important parameters in the solution for U_1 are βh and $T_s\beta/\rho F_a$. The parameter F_a/ω sets the scale of the infragravity velocity and becomes

important when we superpose U_1 with U_0 to determine the total solution for the short-wave-averaged combined current and infragravity wave velocity profiles. In addition, the phase of the surface shear stress δ (relative to the forcing for the U_{a1} component) plays an important role in the solution.

In the surf-zone, Svendsen *et al.* (1987) found (see also Okayasu *et al.* 1988)

$$\nu_t \sim 0.01 h\sqrt{gh} \tag{39}$$

to be a reasonable estimate of the eddy viscosity. Using this we get

$$\beta h \sim \sqrt{\frac{\pi}{0.01}}\sqrt{\left(T\sqrt{g/h}\right)^{-1}} \tag{40}$$

Since $T\sqrt{g/h} \sim 100$ for long waves at typical group periods this means that a typical value for βh is

$$\beta h = O(1) \tag{41}$$

As mentioned earlier, the parameter β is analogous to the similar parameter encountered while dealing with traditional wave boundary layers – it controls the vertical extent to which the effects of the bed and surface shear stresses are felt. The length scale (or "boundary layer thickness") is typically given by $1/\beta$. In traditional wave boundary layers we typically have $\beta h \gg 1$ which means a length scale much smaller than the depth (the boundary layers are thin compared to the depth). In the present case, since $\beta h = O(1)$ we can expect the "boundary layer thickness" to be comparable to the water depth. Particularly, the surface shear stress due to wave grouping affects the long wave velocity profile over the entire depth.

The value of $T_s\beta/\rho F_a$ represents the ratio of the surface shear stress to the depth uniform forcing F_a. The shear stress at mean water level ($z = \overline{\zeta_0}$) is given by (Sitve & Wind 1986)

$$\tau_s = \frac{1}{2}\rho g \frac{\partial \overline{\eta^2}}{\partial x} \tag{42}$$

where η is the free surface elevation with respect to the mean water level (see figure 1). Therefore,

$$\tau_{s1} = \frac{1}{2}\rho g \left(\frac{\partial \overline{\eta^2}}{\partial x}\right)_1 \tag{43}$$

or

$$T_s = \frac{1}{2}\rho g \left| \left(\frac{\partial \overline{\eta^2}}{\partial x}\right)_1 \right| \tag{44}$$

As (44) shows, the value of T_s and therefore $T_s\beta/\rho F_a$ depends on the variation of $\overline{\eta^2}$ at the group period. This variation depends on the amount of groupiness in the short waves at the point in the surf-zone considered. If the groupiness is completely destroyed by the breaking process, then $\overline{\eta^2}$ will be independent of time and $T_s = 0$. If, on the other hand, some groupiness survives the breaking process, $\overline{\eta^2}$ will have a contribution at the group period (*i.e.*, $T_s \neq 0$) in addition to the steady part. Hence, the parameter $T_s\beta/\rho F_a$ measures the ratio between local long wave generation by local wave groupiness (represented by T_s and the $\overline{(u_w \partial u_w/\partial x)_1}$ and the already existing long wave motion represented by $\partial\overline{\zeta_1}/\partial x$ in F_a (see equation 20)).

Relatively little information is presently available on the amount of groupiness that survives the breaking process. List (1991) analyzed field data and found that there is a substantial amount of grouping present in broken waves though it is somewhat reduced by the breaking process. Veeramony (1993) measured surface elevations at different surf-zone locations for incident wave groups in a laboratory wave flume. A representative example of his measurements inside the surf-zone are reproduced in figure 2. This figure clearly shows that in this experiment almost all of the groupiness survives the breaking process. The two measurements cited above suggest that a substantial amount of groupiness survives the breaking process. Thus, quantities like $\overline{\eta^2}$ can be expected to have a contribution at the group period.

The value of T_s may be determined by assuming that a certain amount of groupiness exists in the surf-zone. At any point the total surface elevation $\eta(x,t)$ may be written as follows

$$\eta(x,t) = \frac{A(x,t)}{2} \exp i(\int k dx - \omega_s t) + * \tag{45}$$

where '$*$' represents a complex conjugate and ω_s refers to the short wave frequency. The amplitude A varies over a timescale of the group period and is given by

$$A = a\left(\exp\frac{i\theta}{2} + \epsilon \exp\frac{-i\theta}{2}\right) \tag{46}$$

where a is the mean amplitude of the short waves, ϵ is the groupiness (or modulation) parameter ($(a_{max} - a)/a$, where a_{max} is the maximum wave amplitude in the group) and θ is the phase of the group motion given by

$$\theta = \int \frac{\omega}{c_g} dx - \omega t \tag{47}$$

where c_g is the group velocity and ω is the group frequency. Assuming for simplicity that $a = \gamma h$

inside the surf-zone

$$\left(\overline{\eta^2}\right)_1 = \gamma^2 h^2 \epsilon \cos\theta \tag{48}$$

This leads to

$$\frac{\partial \left(\overline{\eta^2}\right)_1}{\partial x} = \gamma^2 \epsilon h \left(2h_x \cos\theta - \frac{\omega h}{c_g} \sin\theta\right) \tag{49}$$

Using $T\sqrt{g/h} \sim 100$ we find that $\omega h/c_g \sin\theta \sim 0.06$ which is comparable in size to the first term in (49). Therefore, a relevant estimate for (49) is

$$|\frac{1}{2}\frac{\partial \left(\overline{\eta^2}\right)_1}{\partial x}| \sim \gamma^2 \epsilon h h_x \tag{50}$$

which means that the magnitude of the surface shear stress is given by

$$T_s \sim \rho g \gamma^2 \epsilon h h_x \tag{51}$$

The parameter $T_s\beta/\rho F_a$ also contains the forcing F_a which by virtue of (21) contains the modulation of the short-wave-averaged surface elevation as well as the short-wave induced velocity. The latter, once again, depends on the group structure of the short waves in the surf-zone and may be estimated by assuming

$$u_w = c\frac{\eta}{h} \tag{52}$$

which leads to

$$\frac{\partial \overline{u_{w1}^2}}{\partial x} = \frac{g}{h}\left(\frac{\partial \left(\overline{\eta^2}\right)_1}{\partial x} - \frac{\overline{\eta^2}_1 h_x}{h}\right) \tag{53}$$

which, in turn, leads to the following result for $(\partial \overline{u_w^2}/\partial x)_1$

$$|\frac{\partial \overline{u_{w1}^2}}{\partial x}| \sim g\gamma^2 \epsilon h h_x \tag{54}$$

Finally we evaluate the magnitude of db_a/dx based on the results presented by Symonds *et al.* (1982) and Schaffer & Svendsen (1988). These results suggest that for a 10% modulation in wave height ($\epsilon = 0.1$) we get

$$\frac{db_a}{dx} \sim 0.2\frac{d\overline{\zeta_0}}{dx} \sim 0.02 h_x \tag{55}$$

where the latter result follows from Bowen *et al.* (1968) who showed that $d\overline{\zeta_0}/dx \sim 0.1 h_x$ inside the surf-zone. This result was later confirmed by Svendsen *et al.* (1987).

The quantities estimated above indicate (for $\epsilon = 0.1$)

$$F_a \sim 0.02gh_x \tag{56}$$

and

$$\frac{T_s\beta}{\rho F_a} \sim \beta h \tag{57}$$

Finally, the phase of the surface shear stress τ_s relative to the depth uniform forcing F_1 turns out to play an important part in the results presented below. The allowable values for this phase difference depend on magnitudes of $\partial\overline{\zeta}_1/\partial x$ and $\partial\overline{\eta^2}_1/\partial x$. If the $\partial\overline{\eta^2}_1/\partial x$ term dominates over the $\partial\overline{\zeta}_1/\partial x$ term then the phase difference between the depth uniform forcing and the surface shear stress will be small. Physically, this corresponds to a situation where there is a weak long wave component but strong groupiness in the short waves. Clearly, that can happen only locally as the groupiness of the short waves will generate long waves.

If, on the other hand, both terms are of comparable magnitude or if the $\partial\overline{\zeta}_1/\partial x$ term dominates then the shear stress τ_s can have any phase relative to the depth uniform forcing. Since the long wave is reflected from the shoreline, it is similar to a standing wave. The short wave groups, on the other hand, are progressive. Therefore, it follows that the phase difference between the two will change with position. Hence, different values of the phase difference between the infragravity surface elevation and the surface shear stress (which will be in phase with the short wave groups) will correspond to different surf-zone locations. In physical terms, the situation considered in this paragraph is the common one: the wave motion is a combination of short waves with groupiness and long waves.

4.2 Velocity Profiles

Figure 3 presents the variation of the velocity profiles in the surf-zone for the infragravity waves alone in a case with very weak grouping. The parameter values used are $\sqrt{2}T_s\beta/\rho F_a = 0.01$ and $\beta h = 1.5$. Hence, the profiles presented in figure 3 correspond to velocity profiles of infragravity waves in a wave system that either has been regular throughout (long waves generated far away) or where the groupiness has been destroyed at the break point (*e.g.*, the process suggested by Symonds *et al.* (1982)). Figure 3 shows the variation, over half an infragravity wave period, of the long wave velocity profiles for the case when the surface shear stress is in phase with the

depth uniform forcing ($\delta = \pi/2$). The profiles for other values of phase difference are virtually the same as those shown in figure 3 and are hence omitted here. This is not surprising since for the parameter values used, the surface shear stress is negligible in comparison to the depth uniform forcing and hence the phase of the surface shear stress τ_{s1} has no discernible effect on the solution. Consequently, the infragravity velocity profiles have relatively minor variations over depth. The effect of the bottom friction is seen in the reduction of the near bottom velocity. Overall, the profiles presented in figure 3 are in line what we would generally expect to find in long waves with a substantial level of turbulence.

In addition to the infragravity velocity determined above, the short waves also induce steady motions (undertow) in the surf-zone. Therefore, the total short-wave-averaged velocity in the surf-zone is a superposition of the velocity under infragravity waves and the undertow. In figure 4 we show a typical undertow profile. This profile is superposed on the infragravity profiles shown in figure 3 to determine the total short-wave-averaged velocity field in the surf-zone. The profiles so determined are shown in figure 5 for one infragravity wave period. A value of $F_a/\omega\sqrt{gh} = 0.10$ was used in these calculations.

In figure 6 we present the infragravity velocity profiles generated by increasing the ratio $\sqrt{2}T_s\beta/\rho F_a$ from 0.01 to 2 so that the velocity profiles would correspond to a situation with both a significant long wave component present and a strong continued local generation of infragravity waves (*i.e.*, local groupiness in the short waves). The profiles are shown for four different values of the relative phase between the surface shear stress and the depth uniform forcing ($0, \pi/3, 2\pi/3$ and π). As suggested towards the end of the last section, different values of the relative phase between the surface shear stress and the depth uniform forcing would correspond to different surf-zone locations. Hence, the profiles shown in figures 6 are representative of different surf-zone locations.

All the profiles shown in figures 6a-d show considerable variation over the depth. Also seen in these figures is a significant difference in the infragravity velocity profiles as the phase difference between the surface shear stress and the depth uniform forcing changes. Figure 6a shows that when the surface shear stress and the depth uniform forcing are in phase, the entire water column is, over most of the infragravity wave period, accelerating in the same direction as the water at the surface. In complete contrast, figure 6d shows that when the surface shear stress is exactly out of

phase with the depth uniform forcing, the water near the surface is almost always accelerating in the opposite direction of the water acceleration near the bed. Since the effect of the surface shear stress is equivalent to an oscillating boundary layer at the surface, only a small fraction of the response at the bottom can be attributed to the surface shear stress and hence the water near the bed is almost always accelerating in a direction given by the depth uniform forcing component. We also notice that the effect of the bottom friction and boundary layer is relatively weak.

Another effect of the surface shear stress and the depth uniform forcing opposing one another at all times is that at every location the water column is being forced in opposite directions and hence the net force on the water column is reduced. This leads to a reduced response as can be seen by the much smaller velocities in general in figure 6d.

The profiles shown in figure 6 would correspond to locally generated (forced) infragravity motions in the surf-zone and by comparing these profiles with those shown in figure 3 which correspond to free infragravity motions we conclude that the velocity profiles under forced infragravity waves differ considerably from those found under free infragravity waves.

Figures 7a-d show the superposition of the steady undertow and the infragravity profiles of figures 6. It is clearly seen from these figures that the short-wave-averaged velocity has substantial temporal variation.

Next, we investigate the effect of βh on the velocity profiles. Shown in figures 8a-c are the velocity profiles for $\beta h = 0.5, 1, 2$ (see figure 6d for $\beta h = 1.5$). These values span the expected range of variation of the parameter βh. Figures 8 show that the parameter βh controls the response of the water column to the forcing. As in the traditional wave boundary layer solution, the parameter βh determines the distance to which the effect of the surface and bed shear stresses are felt. The smaller the value of βh the larger the distance that is influenced by the shear stresses. Thus, figure 8a shows that for $\beta h = 0.5$ ("boundary layer thickness" $2h$) the surface shear stress influences the solution over the entire water column. For example, for $\pi/10 \leq \omega t \leq 9\pi/10$ the entire water column is accelerating in the same direction as the surface indicating that the surface shear stress is dominating the response. For $\beta h = 1$ figure 8b shows a similar feature only for $2\pi/5 \leq \omega t \leq 7\pi/10$. Thus the influence of the surface shear stress is less strong in this case. For $\beta h = 2$ (figure 8c), the water near the bed is always accelerating in the opposite direction to the acceleration at the surface indicating that the influence of the surface shear stress is very weak

near the bed. Note that large values of βh correspond to situations we are accustomed to from ordinary wave situations (thin boundary layers).

The velocity profiles presented above are of a generic nature. To the best of our knowledge, there are presently no measurements available for the vertical structure of the velocity profiles under infragravity waves. The predicted vertical structure of the forced long waves in the surf-zone are so different from classical long wave theory that these results seem to warrant presentation and discussion even without experimental data. It is hoped that the results presented above will motivate measurements of velocity structure under infragravity waves.

4.3 The Dispersion Coefficient

As mentioned in the introduction and section 2, the cross-shore distribution of the longshore velocity is controlled by the dispersion coefficient D_c, defined by (5), even in a situation with regular waves. As (5) indicates, this dispersion coefficient depends crucially on the vertical distribution of the cross-shore velocity. The expression (5) essentially gives an instantaneous value of D_c. Hence, the results found above for time varying cross-shore currents (infragravity velocities superposed on the undertow) implies that D_c can be expected to vary significantly over an infragravity wave period.

The variation of D_c over an infragravity wave period for the two cases considered above are shown in figure 9. For reference, the steady dispersion coefficient corresponding to the undertow profile shown in figure 4 is also included in this figure. The curves in figure 9 show that in both cases D_c varies considerably over an infragravity wave period. As could also be expected, the variability in D_c is larger for the infragravity profiles corresponding to $T_s\beta/\rho F_a = \sqrt{2}$. In that case, the dispersion coefficient is also found to have much more temporal variation when the surface shear stress is in phase with the depth uniform forcing than compared to the case where the shear stress is out of phase with the depth uniform forcing. When the shear stress is opposing the depth uniform forcing, the temporal variation of D_c is relatively mild. D_c is proportional to the square of the short-wave-averaged velocity and, as figures 7 demonstrate, the short-wave-averaged velocities are both much higher and have more temporal variability in the case when the surface shear stress is in phase with the depth averaged forcing. This, in turn, leads to a much larger variability in time for the dispersion coefficient.

Thus, there is considerable temporal variation of D_c inside the surf-zone. Furthermore, the average value of D_c over an infragravity wave period is always somewhat higher than the dispersion coefficient calculated using the steady undertow. This is because when D_c essentially is proportional to U^2. Finally, since the phase difference between the surface shear stress and the depth uniform forcing varies with position inside the surf-zone, the results shown in figure 9 may be taken to indicate a variation with position of the nondimensional dispersion coefficient.

Since the dispersion coefficient controls the cross-shore distribution of longshore velocities of the infragravity wave motion, the results above indicate that the temporal and spatial variations of D_c are important in the proper modelling of phenomena like forced edge waves. This implies that the inviscid theory normally used to analyze edge waves may not be accurate inside the surf-zone if the edge waves are locally forced. To the authors' knowledge this has not been discussed in the literature.

Also (4) indicates that temporal variations in D_c could force higher harmonics of alongshore infragravity motion. This is in itself not surprising because the dispersive terms arise from the nonlinear interaction of cross-shore and alongshore short-wave-averaged velocities. It is well known that such interactions generate higher harmonics.

5 Summary and Conclusions

In this paper we have presented an analysis of the vertical variation of the particle velocity in periodic infragravity motion. The study has been limited to the simple case of surf-beat due to normally incident wave groups on a long beach. The results, however, can readily be extended to arbitrary wave current situations.

An analytical solution was derived for the velocity profiles under free and forced infragravity waves. These profiles were then superposed on a typical undertow profile inside the surf-zone to determine the combined long wave and current velocity inside the surf-zone. The resulting short-wave-averaged velocity profiles were also used to calculate the temporal variation of the dispersion coefficient D_c.

The results show that the vertical structure of the velocity profiles depends strongly on whether

the infragravity waves are free or forced. Under free infragravity waves the velocity profiles show relatively minor variations over depth and are generally in line with what one expects in long waves. Forced infragravity velocity profiles, on the other hand, show substantial vertical structure.

The dispersion coefficient which controls the cross-shore distribution of the longshore infragravity velocity field was shown to have substantial variation over the period of the infragravity waves all across the surf-zone. In the region where the infragravity motion is forced, the nondimensional dispersion coefficient was found to also have a substantial spatial variation.

These findings may be expected to have a profound effect on many infragravity and current motions in the surf-zone. In particular, it is conjectured that the local temporal variation of the dispersion coefficient will lead to the generation of higher harmonics of infragravity motions with longshore velocity components (edge waves). These results indicate that the spatial and temporal variations of the dispersion coefficient may become important in the modelling of the cross-shore distribution of edge waves.

Acknowledgements

This work is a result of research sponsored by NOAA Office of Sea Grant, Department of Commerce, under Grant No. NA86AA-D-SG040 (Project No. R/OE-6). The U.S. Government is authorized to produce and distribute reprints for government purposes notwithstanding any copyright notation that may appear herein.

Appendix

In this appendix we derive the solutions to equations 26 and 29 subject to (27) and (28) and (30) and (31) respectively. We first deal with the solution for the U_{a2} problem.

Introducing $\xi = z + h_0$ we can write the general solution for (26) as

$$U_{a2} = A \sin[\beta(1+i)\xi] + B \cos(\beta(1+i)\xi] \tag{58}$$

where $\beta = \sqrt{\omega/2\nu_t}$. (28) implies that $A = 0$. (27) gives

$$\frac{T_s}{\rho} \exp(-i\delta) = -\nu_t \beta(1+i) B \sin[\beta(1+i)h] \tag{59}$$

If we let $B = |B|\exp(i\phi_B)$, we get, after some straightforward algebra,

$$|B| = \frac{T_s}{\rho\nu_t\beta\sqrt{2}A_s} \tag{60}$$

$$\phi_B = -\left(\delta + \frac{5\pi}{4} + \phi_s\right) \tag{61}$$

where

$$A_s = \sqrt{\sin^2(\beta h) + \sinh^2(\beta h)} \tag{62}$$

$$\phi_s = \tan^{-1}\left[\frac{\tanh(\beta h)\cos(\beta h)}{\sin(\beta h)}\right] \tag{63}$$

Returning to z for the vertical coordinate and introducing

$$F_2(z) = \frac{\sqrt{\cos^2\left[\beta(z+h_0)\right] + \sinh^2\left[\beta(z+h_0)\right]}}{A_s} \tag{64}$$

$$\phi_{z2}(z) = \tan^{-1}\left\{\frac{-\tanh\left[\beta(z+h_0)\right]\sin\left[\beta(z+h_0)\right]}{\cos\left[\beta(z+h_0)\right]}\right\} \tag{65}$$

we can write the solution for U_{a2} as

$$U_{a2} = \frac{T_s}{\rho\nu_t\beta\sqrt{2}}F_2(z)\exp\left[i\left(\phi_B + \phi_{z2}\right)\right] \tag{66}$$

and $U_{r2} = Re\left\{U_{a2}\exp(-i\omega t)\right\}$ is given by

$$U_{r2} = \frac{F_a}{\omega}\left\{\frac{\sqrt{2}T_s\beta}{\rho F_a}F_2(z)\cos\left[\omega t - \phi_B - \phi_{z2}\right]\right\} \tag{67}$$

which completes the solution for U_{r2}. The term in the parenthesis on the RHS of (67) depends only on the parameters $T_s\beta/\rho F_a$ and βh.

We now turn to the solution for U_{r3}. The solution procedure is similar to the one given above. Introducing $z_1 = z - \overline{\zeta_0}$ we write the general solution to (29) as

$$U_{a3} = C\sin\left[\beta(1+i)z_1\right] + D\cos\left[\beta(1+i)z_1\right] \tag{68}$$

The boundary condition at the surface gives $C = 0$. Introducing $E = f_w u_0/(2\nu_t)$ and writing $U_{a1} + U_{a2}(z = -h_0) = U_{1b}\exp(-i\delta_B)$ the boundary condition at the bed gives

$$D\left\{\beta(1+i)\sin\left[\beta(1+i)h\right] - E\cos\left[\beta(1+i)h\right]\right\} = EU_{1b}\exp(-i\delta_B) \tag{69}$$

Writing $D = |D|\exp(i\phi_D)$ and introducing

$$F_B^2 = 2\left[\sin^2(\beta h) + \sinh^2(\beta h)\right] + \frac{E^2}{\beta^2}\left[\cos^2(\beta h) + \sinh^2(\beta h)\right] + \frac{E}{\beta}\sinh(2\beta h) - \frac{E}{\beta}\sin(2\beta h) \tag{70}$$

$$\phi_F = \tan^{-1}\left[\frac{\sin(\beta h)\cosh(\beta h) + \sinh(\beta h)\cos(\beta h) + \frac{E}{\beta}\sin(\beta h)\sinh(\beta h)}{\sin(\beta h)\cosh(\beta h) - \sinh(\beta h)\cos(\beta h) - \frac{E}{\beta}\cos(\beta h)\cosh(\beta h)}\right] \tag{71}$$

we get

$$|D| = \frac{EU_{1b}}{\beta F_B} \tag{72}$$

$$\phi_D = -(\delta_B + \phi_F) \tag{73}$$

Therefore, the solution for U_{a3} may be written as

$$U_{a3} = \frac{F_a}{\omega}\left\{\frac{f_w u_0}{2\nu_t \beta}\frac{\omega}{F_a} U_{1b} F_3(z) \exp i\left[\phi_D + \phi_3(z)\right]\right\} \tag{74}$$

where

$$F_3(z) = \frac{\sqrt{\cos^2\left[\beta(z-\overline{\zeta_0})\right] + \sinh^2\left[\beta(z-\overline{\zeta_0})\right]}}{F_B} \tag{75}$$

$$\phi_3(z) = \tan^{-1}\left\{\frac{-\sin\left[\beta(z-\overline{\zeta_0})\right]\tanh\left[\beta(z-\overline{\zeta_0})\right]}{\cos\left[\beta(z-\overline{\zeta_0})\right]}\right\} \tag{76}$$

The above gives the following solution for $U_{r3} = Re\left\{U_{a3}\exp(-i\omega t)\right\}$

$$U_{r3} = \frac{F_a}{\omega}\left\{\frac{f_w u_0}{2\nu_t \beta}\frac{\omega}{F_a} U_{1b} F_3(z) \cos\left[\omega t - \phi_D - \phi_3(z)\right]\right\} \tag{77}$$

The solution for U_{r3} is now complete. It is clear that since both U_{a1} and U_{a2} are proportional to F_a/ω, $U_{1b} \propto F_a/\omega$ and therefore the term in the parenthesis of (77) is independent of F_a/ω. If we assume that $u_0 \propto \sqrt{gh}$ and $\nu_t \propto h\sqrt{gh}$ (which are reasonable inside the surf-zone) we find that the parenthetic term above depends only on βh and short wave characteristics.

References

Bowen, A. J., D. L. Inman and V. P. Simmons, 1968, Wave 'set-down' and set-up. Journal of Geophysical Research, 73, pp. 2569-2577

Dally, W. R. and R. G. Dean, 1984. Suspended sediment transport and beach profile evaluation. Journal of Waterway, Port, Coastal and Ocean Engineering, ASCE, 110, pp. 15-33.

Davies, A. M., 1987. On extracting current profiles from vertically integrated numerical models. Coastal Engineering, 11, pp. 445-477.

deVriend, H. J. and M. J. F. Stive, 1987. Quasi-3D modelling of nearshore currents. Coastal Engineering, 11, pp. 565-601.

Elgar, S., T. H. C. Herbers, M. Okihiro, J. Oltman-Shay and R. T. Guza, 1992. Observations of infragravity waves. Journal of Geophysical Research, 97, pp. 15573-15577.

Guza, R. T. and E. B. Thornton, 1982. Swash oscillations on a natural beach. Journal of Geophysical Research, 87, pp. 483-491.

Guza, R. T. and E. B. Thornton, 1985. Observations of surf beat. Journal of Geophysical Research, 90, C2, pp. 3161-3171.

Herbers, T. H. C., S. Elgar, R. T. Guza and W. C. O'Riley, 1992. Infragravity frequency motions on the shelf. Proceedings of the 23rd Coastal Engineering Conference, pp. 846-859

Howd, P. A., J. Oltman-Shay and R. A. Holman, 1991. Wave variance partitioning in the trough of a barred beach. Journal of Geophysical Research, 96, pp. 12781-12795.

Huntley, D. A., R. T. Guza and E. B. Thornton, 1981. Field observations of surf beat, Part I: Progressive edge waves. Journal of Geophysical Research, 86, pp. 6451-6466.

Jin, X. and C. Kranenburg, 1993. Quasi 3D numerical modeling of shallow-water circulation. Journal of Hydraulic Engineering, vol. 119, no. 4, pp. 458-472.

List, J. H., 1991. Wave groupiness in the nearshore. Coastal Engineering, 15, pp. 475-496.

List, J. H., 1992. A model for the generation of two dimensional surf beat. Journal of Geophysical Research, 97, C4, pp. 5623-5635.

Longuet-Higgins, M. S., 1953. Mass transport in water waves. Philosophical Transactions of the Royal Society, 345, pp. 5355-581.

Longuet-Higgins, M. S. and R. W. Stewart, 1962. Radiation stress and mass transport in gravity waves with application to 'surf-beats'. Journal of Fluid Mechanics, 8, pp. 565-583.

Longuet-Higgins, M. S. and R. W. Stewart, 1964, Radiation stress in water waves, a physical discussion with application. Deep Sea Research, 11, pp. 529-563.

Mei, C. C. 1983. The applied dynamics of ocean surface waves. John Wiley and Sons, New York, 740 pp.

Munk, W. H., 1949. Surf beats. Transactions of the American Geophysical Union, 30, pp. 849-854.

Okayasu, A., T. Shibayama and K. Horikawa, 1988. Vertical variation of undertow in the surf-zone. Proceedings of the 21st Coastal Engineering Conference, pp. 478-491.

Oltman-Shay, J. and R. T. Guza, 1987. Infragravity edge wave observations on two California beaches. Journal of Physical Oceanography, 17, pp. 644-663.

Phillips, O. M., 1977. The dynamics of the upper ocean. Cambridge University Press, 336 pp.

Putrevu, U. and I. A. Svendsen, 1992. A mixing mechanism in the nearshore region. Proceedings of the 23rd International Conference on Coastal Engineering, 2758-2771.

Putrevu, U. and I. A. Svendsen, 1993. Vertical structure of the undertow outside the surf-zone. Journal of Geophysical Research, in press.

Roelvink, J. A. and M. J. F. Stive, 1988. Bar generating cross-shore flow mechanisms on a beach. Journal of Geophysical Research, 94, pp. 4785-4800.

Schaffer, H. A., 1993. Infragravity waves induced by short-wave groups. Journal of Fluid Mechanics, 247, pp. 551-588.

Schaffer, H. A. and I. A. Svendsen, 1988. Surf beat generation on a mild slope beach. Proceedings of the 21st International Conference on Coastal Engineering, pp. 1058-1072.

Stive, M. J. F. and H. G. Wind, 1986. Cross-shore mean flow in the surf-zone. Coastal Engineering, 10, pp. 325-340.

Svendsen, I. A., 1984. Mass flux and undertow in a surf-zone. Coastal Engineering, 8, pp. 347-365.

Svendsen, I. A. and J. B. Hansen, 1988. Cross-shore currents in surf-zone modelling. Coastal Engineering, 12, pp. 23-42.

Svendsen, I. A. and R. S. Lorenz, 1989. Velocities in combined undertow and longshore currents. Coastal Engineering, 13, pp. 55-79.

Svendsen, I. A. and Putrevu, U. 1993. Nearshore Mixing and Dispersion. Submitted for publication.

Svendsen, I. A., H. A. Schaffer and J. B. Hansen, 1987. The interaction between the undertow and boundary layer flow on a beach. Journal of Geophysical Research 92, pp. 11,845-856.

Symonds, G. and A. J. Bowen, 1984. Interaction of nearshore bars with incoming wave groups. Journal of Geophysical Research, 89, C2, pp. 1953-1959.

Symonds, G., D. A. Huntley and A. J. Bowen, 1982. Two dimensional surf-beat: Long wave generation by a time-varying break point. Journal of Geophysical Research, 87, pp. 492-498.

Tucker, M. J., 1950. Surf beats: Sea waves of 1 to 5 minute period. Proceedings of the Royal Society of London, A 202, pp. 565-573.

Veeramony, J., 1993. Master's thesis, Department of Civil Engineering, University of Delaware. In preparation.

Wright, L. D., R. T. Guza and A. D. Short, 1982. Dynamics of a high energy dissipative surf-zone. Marine Geology, 45, pp. 41-62.

List of figures

- **Figure 1:** Definition sketch.
- **Figure 2:** Measured group structure inside the surf-zone (from Veeramony 1993).
- **Figure 3:** Infragravity velocity profiles for $\sqrt{2}T_s\beta/(\rho F_a) = 0.01$ and $\beta h = 1.5$.
- **Figure 4:** Typical undertow profile inside the surf-zone.
- **Figure 5:** Total short wave averaged velocity field inside the surf-zone for $\sqrt{2}T_s\beta/(\rho F_a) = 0.01$, $\beta h = 1.5$ and $F_a/(\omega\sqrt{gh}) = 0.1$.
- **Figure 6:** Infragravity velocity profiles for $\sqrt{2}T_s\beta/\rho F_a = 2$ and $\beta h = 1.5$.
- **Figure 7:** Total short wave averaged velocity field inside the surf-zone for $\sqrt{2}T_s\beta/(\rho F_a) = 2$, $\beta h = 1.5$ and $F_a/(\omega\sqrt{gh}) = 0.1$.
- **Figure 8:** Infragravity velocity profiles for $\sqrt{2}T_s\beta/(\rho F_a) = 2$, $\beta h = 0.5, 1, 2$.
- **Figure 9:** Temporal variation of the dispersion coefficient: a) Dispersion coefficient due to steady undertow, b) Dispersion coefficient due to velocity profiles of figure 5, c) Dispersion coefficient due to velocity profiles of figure 7a, d) Dispersion coefficient due to velocity profiles of figure 7b, e) Dispersion coefficient due to velocity profiles of figure 7c and f) Dispersion coefficient due to velocity profiles of figure 7d.

Figure 1

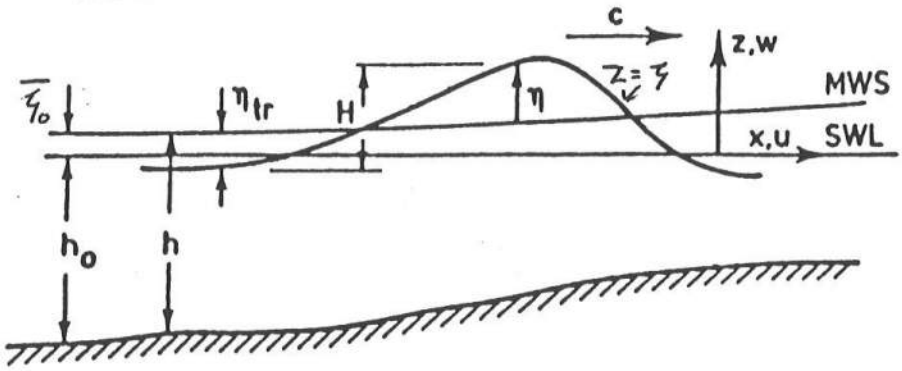

Figure 2

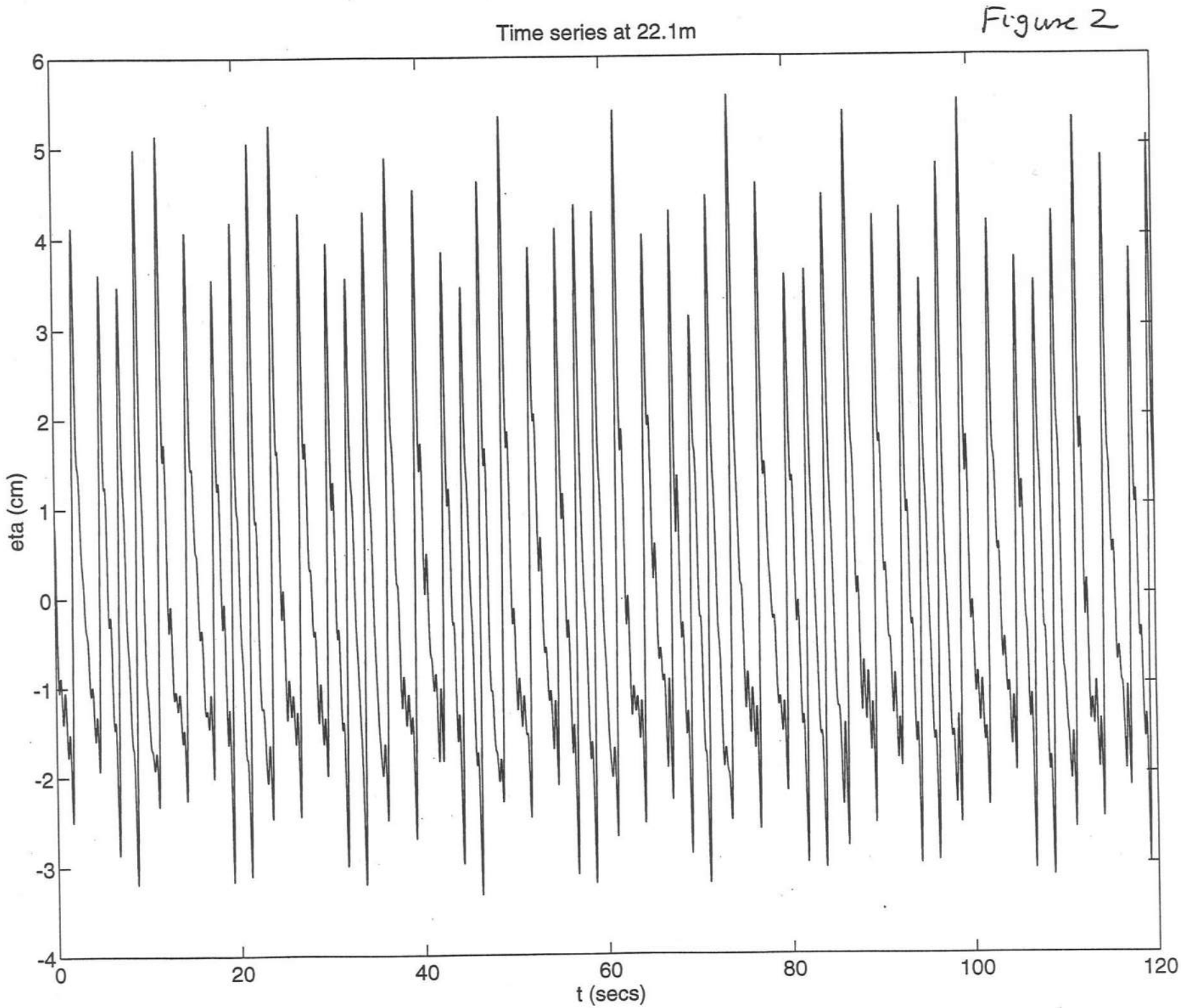
Time series at 22.1m
eta (cm)
t (secs)
6
5
4
3
2
1
0
-1
-2
-3
-4
0
20
40
60
80
100
120

Figure 3

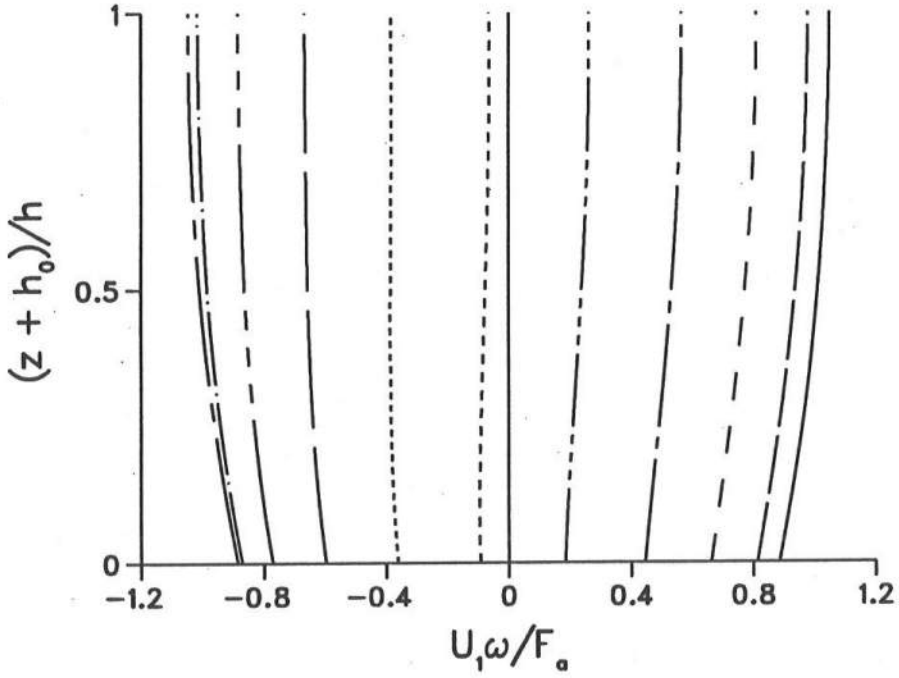

Legend

ω t = 0.000

ω t = 0.314

ω t = 0.628

ω t = 0.942

ω t = 1.257

ω t = 1.571

ω t = 1.885

ω t = 2.199

ω t = 2.513

ω t = 2.827

ω t = 3.142

Figure 4

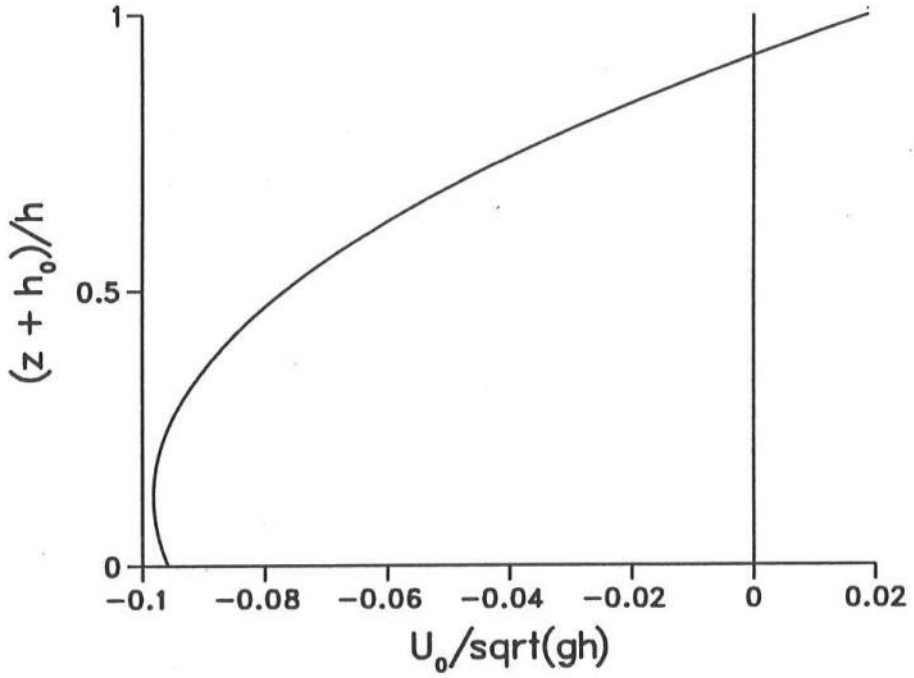

Figure 5

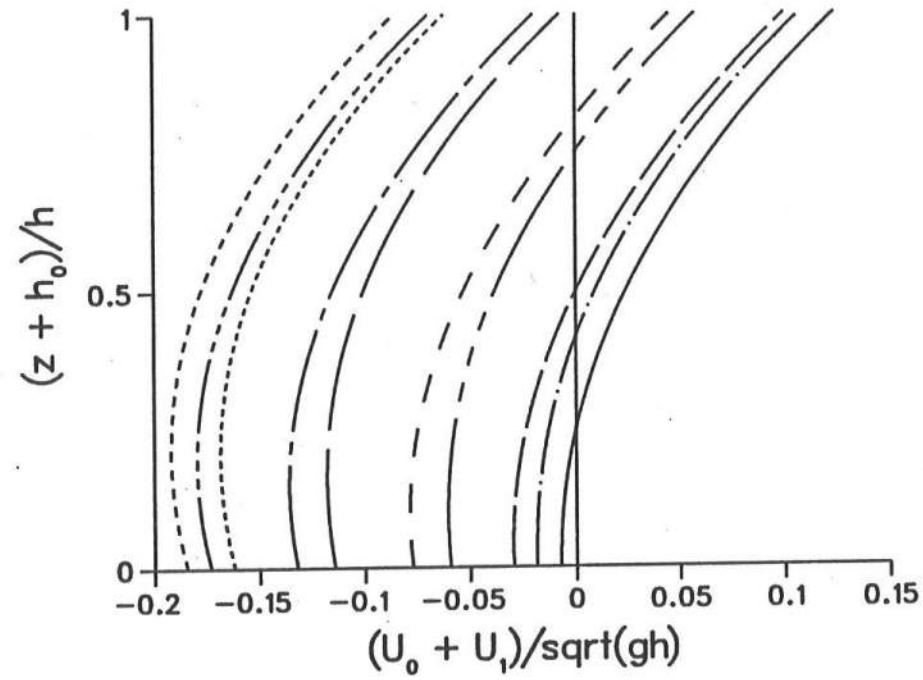

Legend

ω t = 0.000

ω t = 0.628

ω t = 1.257

ω t = 1.885

ω t = 2.513

ω t = 3.142

ω t = 3.770

ω t = 4.398

ω t = 5.027

ω t = 5.655

ω t = 6.283

Figure 6a

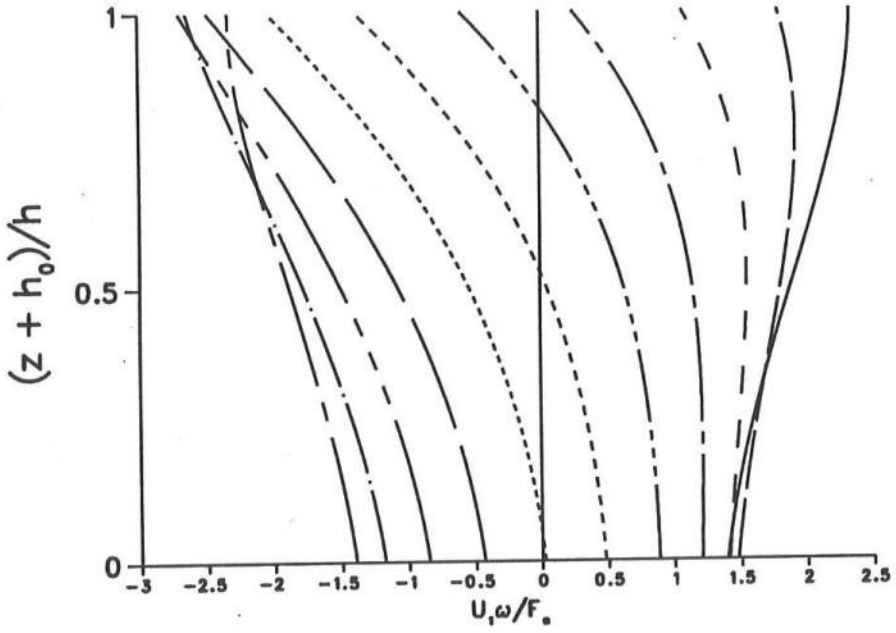

Legend

ω t = 0.000

ω t = 0.314

ω t = 0.628

ω t = 0.942

ω t = 1.257

ω t = 1.571

ω t = 1.885

ω t = 2.199

ω t = 2.513

ω t = 2.827

ω t = 3.142

Figure 6b

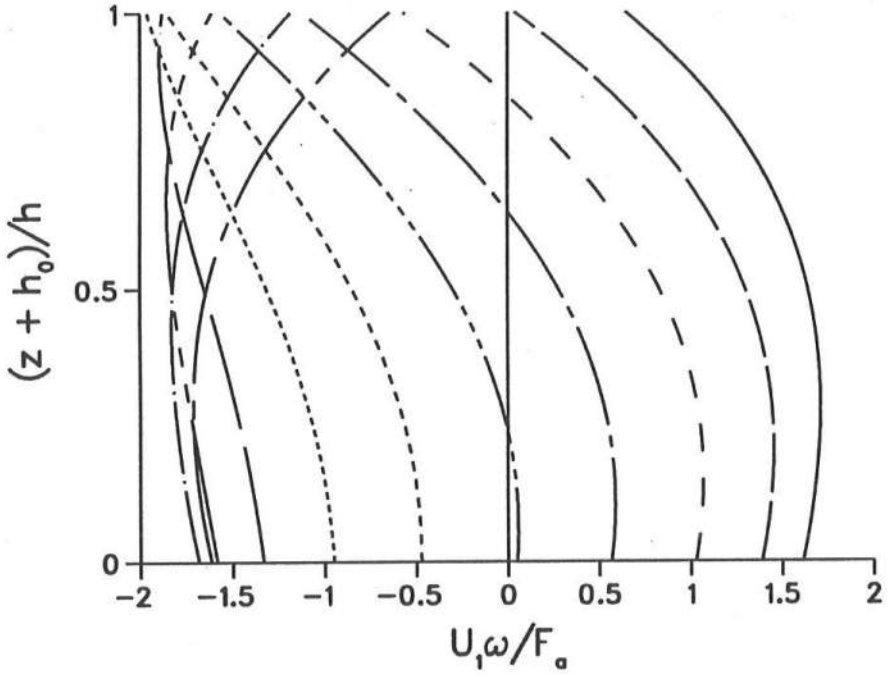

Legend

ω t = 0.000

ω t = 0.314

ω t = 0.628

ω t = 0.942

ω t = 1.257

ω t = 1.571

ω t = 1.885

ω t = 2.199

ω t = 2.513

ω t = 2.827

ω t = 3.142

Figure 6c

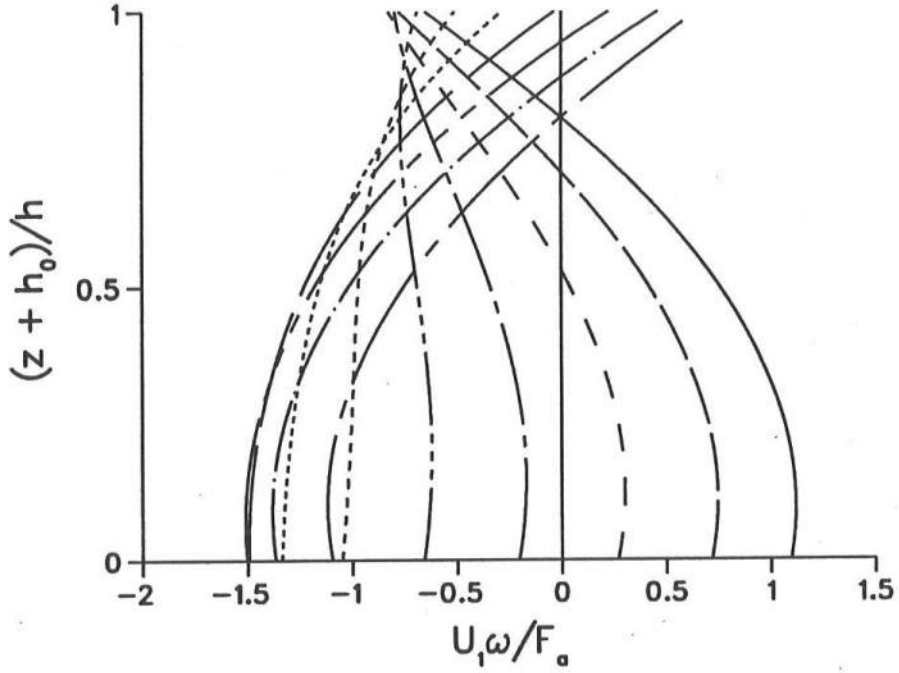

Legend

ω t = 0.000

ω t = 0.314

ω t = 0.628

ω t = 0.942

ω t = 1.257

ω t = 1.571

ω t = 1.885

ω t = 2.199

ω t = 2.513

ω t = 2.827

ω t = 3.142

Figure 6d

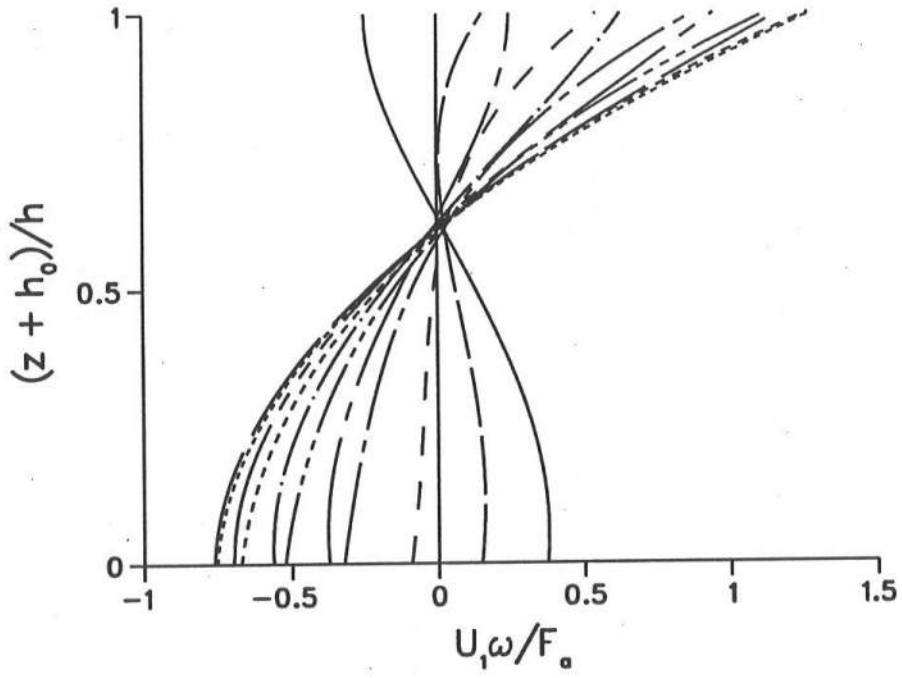

Legend

ω t = 0.000

ω t = 0.314

ω t = 0.628

ω t = 0.942

ω t = 1.257

ω t = 1.571

ω t = 1.885

ω t = 2.199

ω t = 2.513

ω t = 2.827

ω t = 3.142

Figure 7a

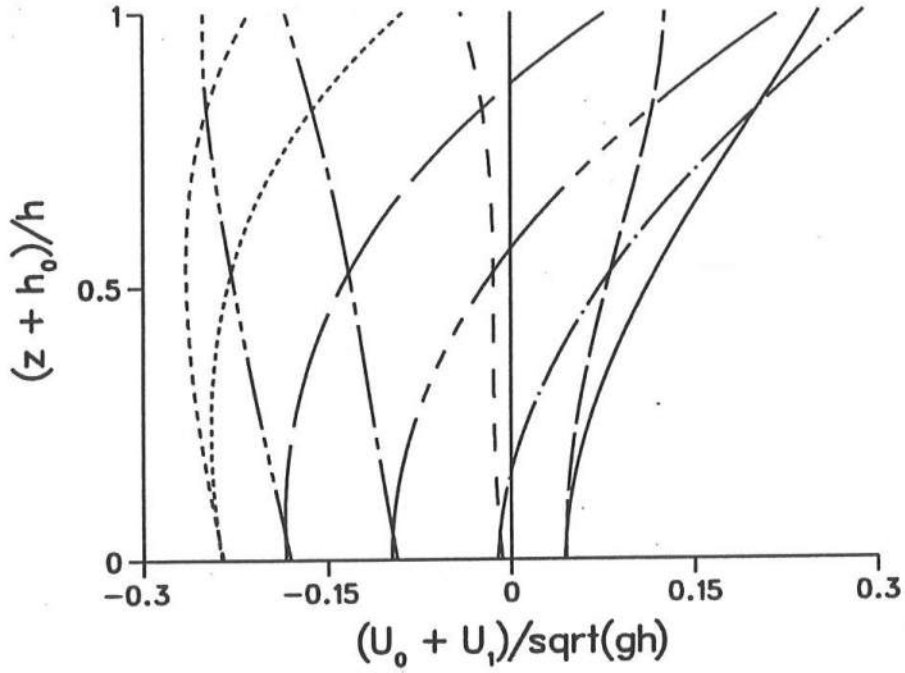

Legend

ω t = 0.000

ω t = 0.628

ω t = 1.257

ω t = 1.885

ω t = 2.513

ω t = 3.142

ω t = 3.770

ω t = 4.398

ω t = 5.027

ω t = 5.655

ω t = 6.283

Figure 7b

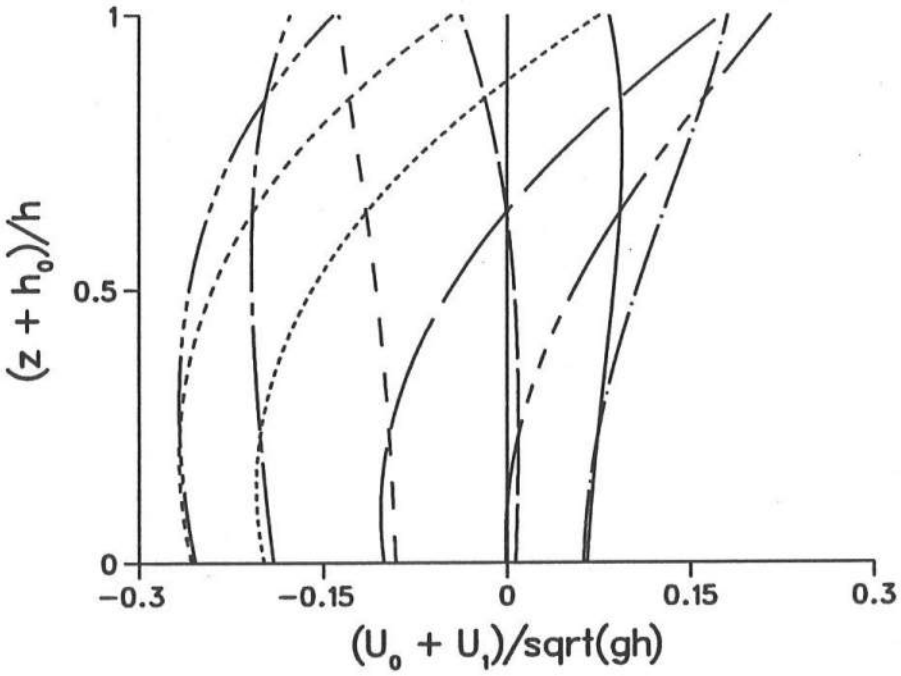

Legend

ω t = 0.000

ω t = 0.628

ω t = 1.257

ω t = 1.885

ω t = 2.513

ω t = 3.142

ω t = 3.770

ω t = 4.398

ω t = 5.027

ω t = 5.655

ω t = 6.283

Figure 7c

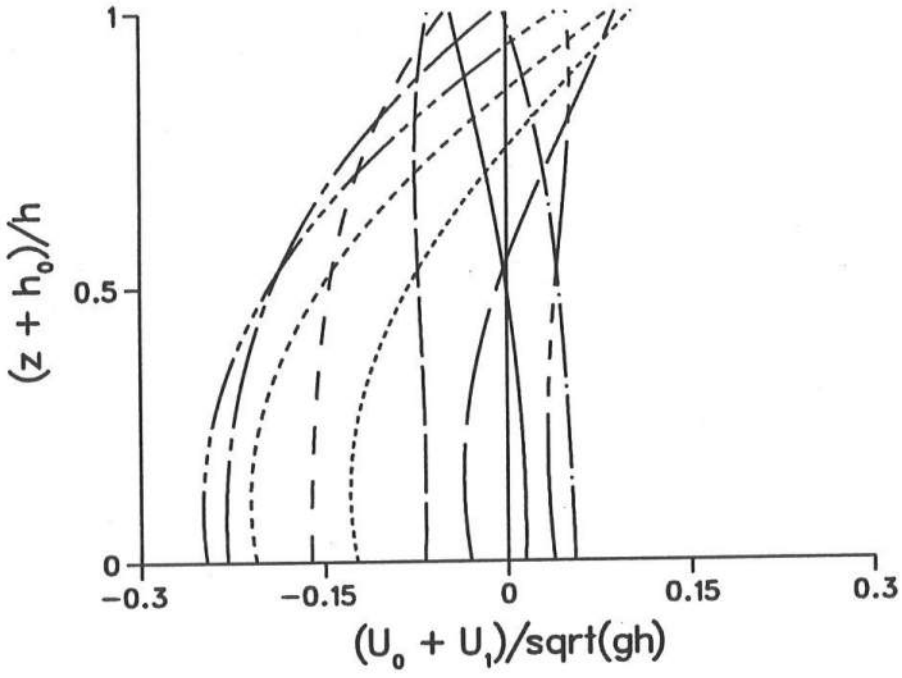

Legend

ω t = 0.000

ω t = 0.628

ω t = 1.257

ω t = 1.885

ω t = 2.513

ω t = 3.142

ω t = 3.770

ω t = 4.398

ω t = 5.027

ω t = 5.655

ω t = 6.283

Figure 7d

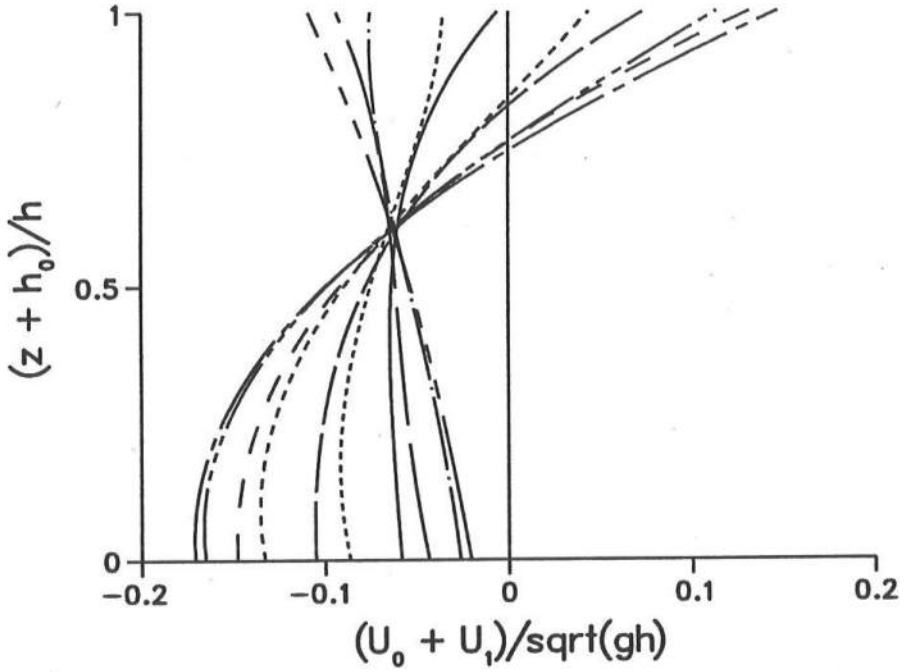

Legend

ω t = 0.000

ω t = 0.628

ω t = 1.257

ω t = 1.885

ω t = 2.513

ω t = 3.142

ω t = 3.770

ω t = 4.398

ω t = 5.027

ω t = 5.655

ω t = 6.283

Figure 8a

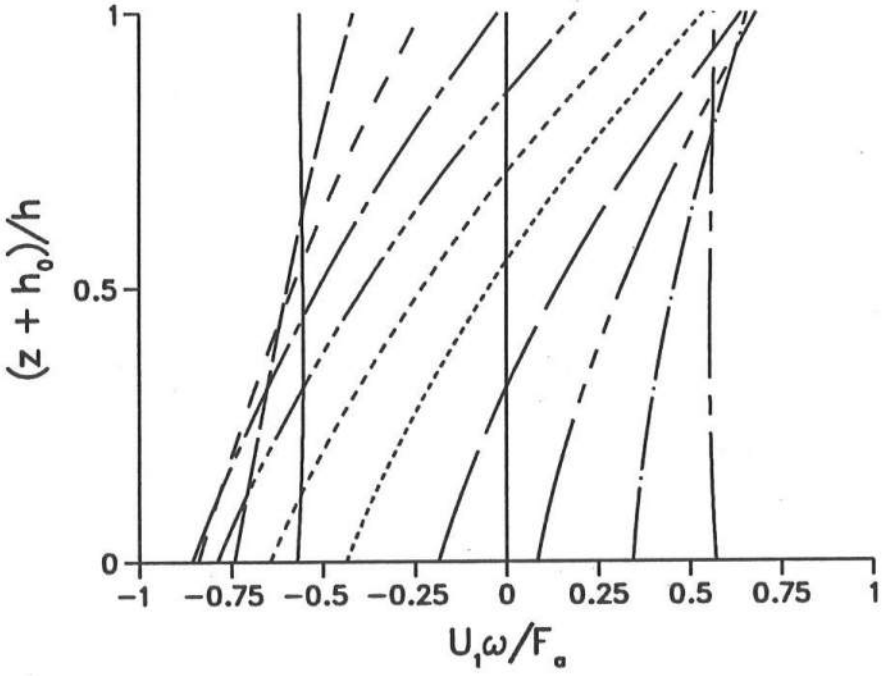

Legend

ω t = 0.000

ω t = 0.314

ω t = 0.628

ω t = 0.942

ω t = 1.257

ω t = 1.571

ω t = 1.885

ω t = 2.199

ω t = 2.513

ω t = 2.827

ω t = 3.142

Figure 8b

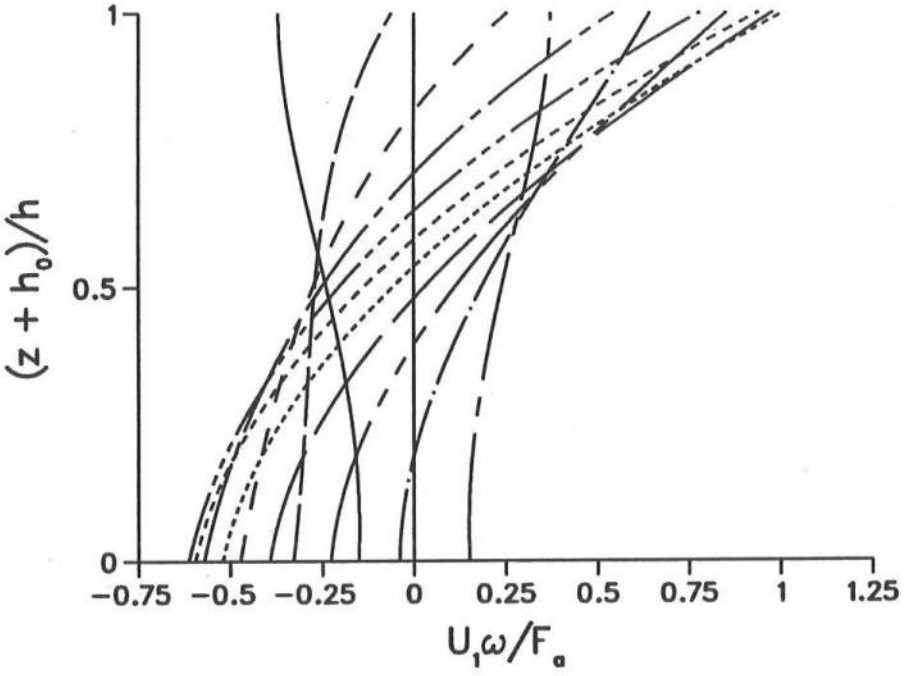

Legend

ω t = 0.000

ω t = 0.314

ω t = 0.628

ω t = 0.942

ω t = 1.257

ω t = 1.571

ω t = 1.885

ω t = 2.199

ω t = 2.513

ω t = 2.827

ω t = 3.142

Figure 8c

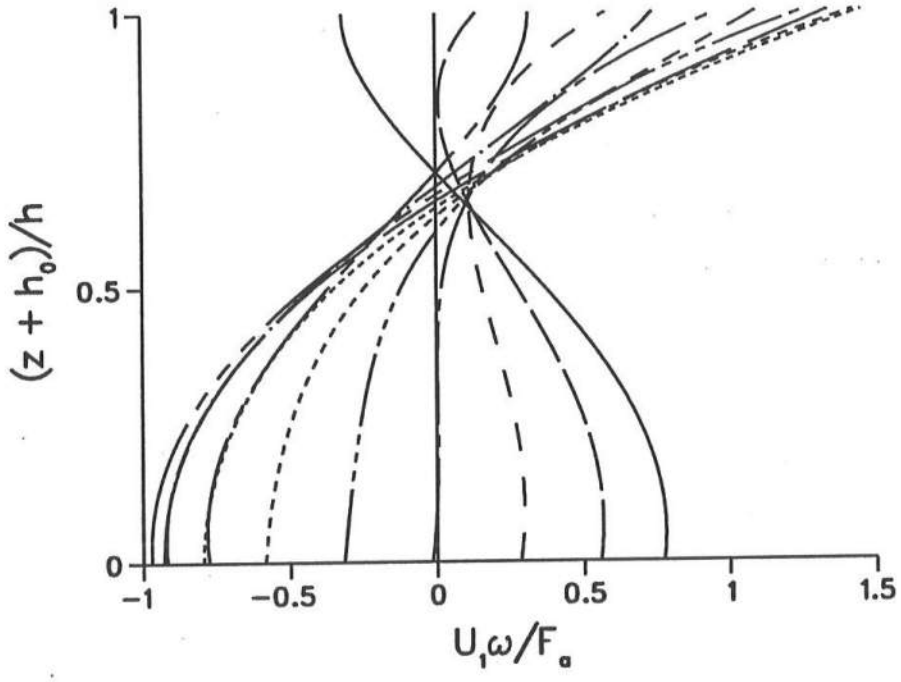

Legend

ω t = 0.000

ω t = 0.314

ω t = 0.628

ω t = 0.942

ω t = 1.257

ω t = 1.571

ω t = 1.885

ω t = 2.199

ω t = 2.513

ω t = 2.827

ω t = 3.142

Figure 9

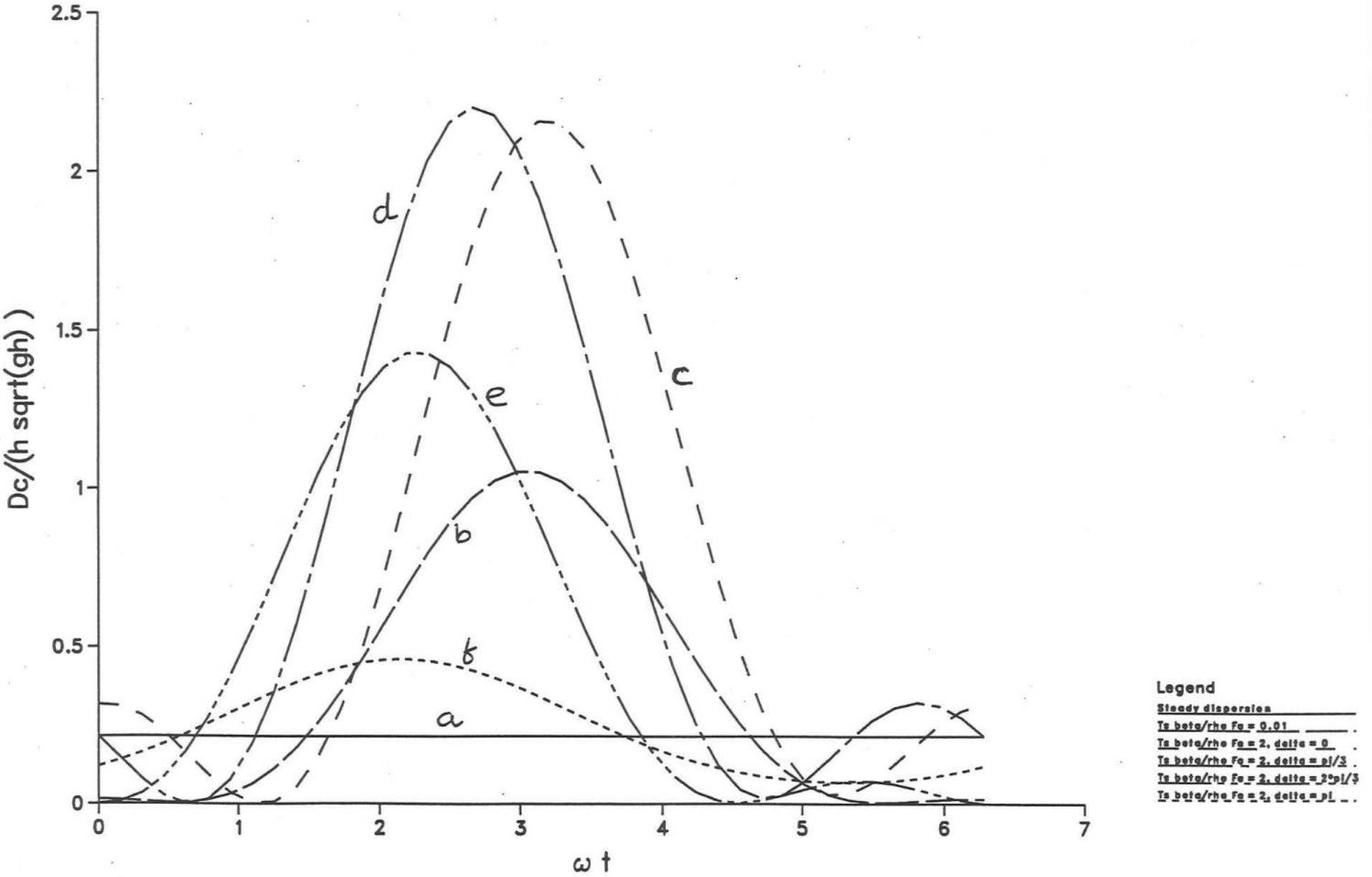
2.5
2
1.5
1
0.5
0
0
1
2
3
4
5
6
7
Dc/(h sqrt(gh))
ω t
a
b
c
d
e
f
Legend
Steady dispersion
Ts beta/rho Fo = 0.01
Ts beta/rho Fo = 2, delta = 0
Ts beta/rho Fo = 2, delta = pi/3
Ts beta/rho Fo = 2, delta = 2*pi/3
Ts beta/rho Fo = 2, delta = pi